Eur J Med Res (2005) 10: 47-55

IMAGE FUSION OF CT AND MRI FOR THE VISUALIZATION OF THE AUDITORY AND VESTIBULAR SYSTEM

M. D. Seemann[1,2], J. Beltle[2], M. Heuschmid[2], H. Löwenheim[3], H. Graf[4], C. D. Claussen[2]

[1]Department of Nuclear Medicine, Technical University, Munich, Germany
[2]Department of Diagnostic Radiology, [3]Department of Otorhinolaryngology, [4]Section on Experimental Radiology, Eberhard-Karls University, Tuebingen, Germany

Abstract: The aim of this study was to perform a realistic visualization of the auditory and vestibular system using volume data sets from high-resolution computed tomography (HR-CT) and high-resolution magnetic resonance imaging (HR-MRI).

In 10 patients with conductive and/or sensorineural hearing loss, vertigo and tinnitus, HR-CT and HR-MRI of the petrous bone were performed consecutively. CT was performed with a 16-slice computed tomography scanner using a high spatial resolution. MRI was perfomed with a 3.0 Tesla scanner using a three-dimensional-constructive interference in steady state (3D-CISS) gradient-echo, and T2-weighted, unenhanced and gadolinium (GD)-enhanced T1-weighted turbo spin-echo sequences. The middle ear structures were interactively segmented and visualized with a color-coded shaded-surface rendering method using the HR-CT volume data sets. The inner ear structures were interactively segmented and visualized with a color-coded shaded-surface rendering method using the high-resolution 3D-CISS MRI volume data sets. Finally, both shaded-surface rendered models were superimposed semi-automatically using a commercial available software program to visualize the auditory and vestibular system.

The representation of the middle and inner ear structures with image fusion of HR-CT and HR-MRI takes advantage of both the high bony contrast of HR-CT and the high soft tissue contrast discrimination and sensitivity to fluids of HR-MRI, as well as the high spatial resolution of both modalities. In comparison to the fused axial CT/MRI, the images of 3D CT/MRI fusion facilitates a clear representation and better spatial orientation.

The middle and inner ear consists of bony structures, soft tissue structures and fluid-filled spaces. For this reason, the image fusion of volume data sets from HR-CT and HR-MRI allowed an optimized and realistic visualization of the auditory and vestibular system.

Key words: Ear, anatomy; Computed tomography (CT), multi-detector row; Computed tomography (CT), image processing; Magnetic resonance (MR), high-field-strength imaging; Magnetic resonance (MR), image processing; Image, fusion

INTRODUCTION

Post-processing of image data sets is an important aspect of interpretation and representation of complex anatomical findings and pathological changes, and it has become more and more important in clinical practice [1]. In recent years much effort has been directed towards improving the capabilities and efficiency of independent workstations to allow the rapid manipulation of imaging data sets and to improve the image quality of post-processing visualization methods.

Since the external and middle ear develop separately from the inner ear, the majority of inner ear malformations occur without any external or middle ear involvement, and vice versa [2]. The diagnosis of diseases of the middle and inner ear is usually based on a variety of subjective and objective clinical symptoms such as hearing loss, vertigo, tinnitus and nystagmus. Although parts of the middle ear and its pathology can be investigated by direct microscopy, the inner ear is not directly accessible to clinical investigation. Patients with chronic infections of the middle ear, conductive hearing loss (CHL), tinnitus, otalgia, otorrhea and facial paresis or paralysis as a result of middle ear disease, post-traumatic CHL or sensorineural hearing loss (SNHL), or recurrent CHL after prosthetic stapedectomy are best depicted by computed tomography (CT) [3-5]. Magnetic resonance imaging (MRI) is accepted as the most sensitive imaging technique in patients with inner ear malformations which present clinically as SNHL, vertigo and tinnitus [2, 3, 6]. Therefore, in the visualization of the auditory and vestibular system and the clarification of congenital malformations, petrous apex lesions, and mixed hearing loss, MRI and CT are complementary [3]. Furthermore, the complicated function of the middle and inner ear is reflected by the complicated spatial anatomy, which can be difficult to conceptualize and interpret from a large number of planar high-resolution computed tomography (HR-CT) or high-resolution magnetic resonance imaging (HR-MRI) images [1]. Abnormalities and pathological alterations also make their interpretation more complicated.

This study aims to show the possibilities and advantages of visualizing the auditory and vestibular system

with image fusion utilising the advantages of both computed tomography (CT) and magnetic resonance imaging (MRI).

Marerials and Methods

Patients

In a four months period, 10 consecutive patients (6 women and 4 men) suffering from conductive and/or sensorineural hearing loss (n = 5), tinnitus (n = 3) and vertigo (n = 2) were examined using high-resolution computed tomography (HR-CT) and high-resolution magnetic resonance imaging (HR-MRI). In each patient, both imaging procedures of the petrous bone were performed as part of a clinical routine examination on the same day. Informed consent was obtained from all patients. The mean age ± SD of the patients was 45.0 ± 16.1 years.

CT Data Acquisition

High-resolution computed tomography (HR-CT) examinations were performed using a 16-slice computed tomography scanner (SENSATION® 16, Siemens Medical Solutions, Erlangen, Germany). A lateral scout-view was obtained for planning and determining the location of the scanning volume. To reduce lens radiation, data acquisition was performed parallel to the hard palate. Scans of the petrous bone were acquired in a cranio-caudal direction using a slice collimation of 16 x 0.75 mm, tube voltage of 120 kV, tube current of 240 mAs, table feed of 12.0 mm (Pitch = 1), rotation time of 1.0 sec and a 512 x 512 matrix. No contrast agent was administered. After data acquisition, the axial images of each side of the petrous bone were reconstructed separately in order to reduce the primary field of view to 60 mm, to decrease pixel size and to provide high spatial resolution using a 0.3 mm increment (voxel size 0.117 x 0.117 x 0.30 mm^3). A 180° interpolation and high-resolution software algorithm were used to emphasize bony details (Kernel U80u very sharp).

MRI Data Acquisition

High-resolution magnetic resonance imaging (HR-MRI) examinations were performed with a 3.0 Tesla MR scanner (MAGNETOM Trio®, Siemens Medical Solutions) using a standard circularly polarized head coil. Initially, to image at high spatial resolution, each inner ear was separately examined using a three-dimensional-constructive interference in steady state (3D-CISS) gradient-echo sequence. The parameters for the 3D-CISS sequence were: repetition time TR = 8.97 msec, echo time TE = 4.64 msec, flip angle α = 48°, acquisition time TA = 7 min 37 sec. The high spatial resolution with a voxel size of 0.39 x 0.39 x 0.40 mm^3 was achieved by selective excitation of an axial slab (thickness 25.6 mm, 64 partitions) and a 256 x 256 matrix for a 100 mm field-of-view. Phase encoding was chosen in antero-posterior direction, and phase oversampling of 25% was necessary to avoid overfolding to the region of the inner ear.

Subsequently, a slice selective technique was used in which a block including 20 axial T2-weighted as well as native and contrast agent enhanced T1-weighted images was recorded with turbo spin-echo (TSE) sequences using the standard protocol parameters as established for inner ear examinations at 1.5 T (for T2-weighting: TR = 4,000 msec, TE = 100 msec and for T1-weighting: TR = 500 msec, TE = 15 msec). Imaging was performed for both inner ears simultaneously using a field-of-view that covered the entire head in cross section. A slice thickness of 2.0 mm and an in-plane resolution of 0.9 x 0.4 mm^2 were used. For contrast agent enhanced imaging, Gd-DTPA was administered intravenously at a concentration of 0.1 mmol/kg bodyweight.

Three-dimensional (3D) Reconstruction

The HR-CT and HR-MRI data sets were transferred to an independent high performance graphic computer (EasyVision 5.1, Philips Medical Systems, Best, The Netherlands). The resolution for HR-CT and HR-MRI were a 512 x 512 matrix and a 256 x 256 matrix, respectively. A color-coded shaded-surface display (SSD) rendering method was used as the post-processing technique, because only this reconstruction method allowed a reliable image fusion of the CT and MRI data sets. The computer program allowed for the magnification of specific regions in the axial images. Each anatomical structures of the middle and inner ear were manually segmented from an researcher by drawing a boundary line using the axial HR-CT and HR-MRI source images, respectively. The voxels within the segmentation area were automatically marked and used to define the corresponding anatomical structure. After complete segmentation, a surface model of the structures of interest was automatically constructed using geometric primitives. The anatomical structures of the auditory and vestibular system were color coded and displayed using a shaded-surface rendering method, such that the degree of transparency of each structure could be varied. Each structure could thus be separately studied in detail as a 3D object, turned about any axis and measured in terms of distance and volume.

Image Fusion

The independent high performance graphic computer (EasyVision 5.1, Philips Medical Systems) was used to register the HR-CT and the 3D-CISS MRI volume data sets using a semiautomatic point-based technique. At least 7 anatomical landmarks had to be placed in the same positions on the axial source images of both imaging modalities. To perform the automatic superimposition of the CT and MRI images, the landmarks had to have a high agreement (at least a 97% coincidence). The superimposed color-coded shaded-surface image fusion method allows the intensity of both studies to be adjusted independently.

Image Interpretation

The examinations were qualitatively evaluated by two experienced observers. They described the middle and

inner ear structures qualitatively with respect to the clarity of the representation in the axial 2D source images of CT (W = 4000 HU; C = 800 HU), axial 2D source images of MRI, the fused axial images of CT/MRI and the fused color-coded SSD images of CT/MRI. Finally, they qualitatively compared the middle and inner ear structures with respect to the clarity of the spatial orientation in the fused axial images of CT/MRI and the fused color-coded SSD images of CT/MRI. Each case was read blindly and independently using a score from 0 to + + + (0 = not visible, + = insufficient, + + = fair, + + + = optimal).

Results

A total of 10 patients were studied with the main emphasis on the image fusion and visualization of the structures of the middle and inner ear using CT and MRI volume data sets. The thin contiguous axial HR-CT (Fig. 1a, 2a) and HR-MRI (Fig. 1c, 2c) scans provided high quality images of the middle and inner ear structures and permited high quality three-dimensional reconstruction. Due to the relatively short scanning times, artifacts resulting from patient movement did not occur.

Using HR-CT, each anatomical structure of the middle ear, including the membrana tympani, the malleus and incus with their ligamentous suspensions, stapes, the musculus stapedius, and the intraosseous part of the facial nerve, could always be separately segmented and coded with its own color. In one patient, a congenital dislocation of the ossicular chain was found. Using HR-MRI, each anatomical structure of the inner ear, including the superior, lateral and posterior semicircular canals, the vestibule, the cochlea with its basilar membrane and the cranial nerves (facial nerve and vestibulocochlear nerve) within the internal auditory canal (IAC) and the cerebellopontine angle (CPA), could always be separately segmented and also coded with its own color. In one patient, an acoustic neurinoma of the internal auditory canal was detected.

The rate-limiting step in the shaded-surface rendering image processing was the segmentation of the anatomical structures of interest. Using the high quality interactive segmentation, up to 25 ± 5 minutes was required for a complete color-coded shaded-surface rendering of the middle (Fig. 1b, 2b) and inner ear structures (Fig. 1d, 2d). The following image fusion of HR-CT and HR-MRI axial source images (Fig. 1e, 2e) required only a few seconds and takes the advantages of both imaging procedures and improve the representation of the auditory and vestibular system (Table 1). In comparison to the fused axial images of CT/MRI, the color-coded shaded-surface rendered image fusion (Fig. 1f, 2f) could display the middle and inner ear structures in their complete form and their correct topographic relationship to critical vascular, neural, and other structures more realistically and improve the spatial orientation (Table 2).

Dicussion

Computed tomography (CT) and magnetic resonance imaging (MRI) are the two most important imaging modalities for evaluation of the auditory and vestibular system as well as their anomalies and pathologies. Each of these modalities has specific advantages and disadvantages, and are therefore complementary imaging techniques. The ability to produce thin sections and high spatial resolution images from CT and MRI data sets are the indispensable prerequisites for detailed morphological analysis of the complicated spatial relationship of the sub-millimeter structures of the middle and inner ear and open up new possibilities for

Table 1. Qualitative assessment of the representation of the middle and inner ear structures (n = 20) in the axial 2D source images of CT and MRI compared with the fused axial CT/MRI (consensus readings).

	axial CT	axial MRI	axial CT/MRI fusion
Middle ear structures			
malleus	+ + +	0	+ + +
incus	+ + +	0	+ + +
stapes	+ + +	0	+ + +
Inner ear structures			
superior semicircular canal	+ + +	+ +	+ + +
lateral semicircular canal	+ + +	+ +	+ + +
posterior semicircular canal	+ + +	+ +	+ + +
vestibule	+ + +	+ + +	+ + +
cochlea	+ + +	+ + +	+ + +
basilar membran	0	+ + +	+ + +
facial nerve			
part in the IAC and CPA	0	+ + +	+ + +
part in the petrous bone	+ +	0	+ +
vestibulocochlear nerve	0	+ + +	+ + +

Note.—Each case was read using a score from 0 to + + + (0 = not visible, + = insufficient, + + = fair, + + + = optimal).

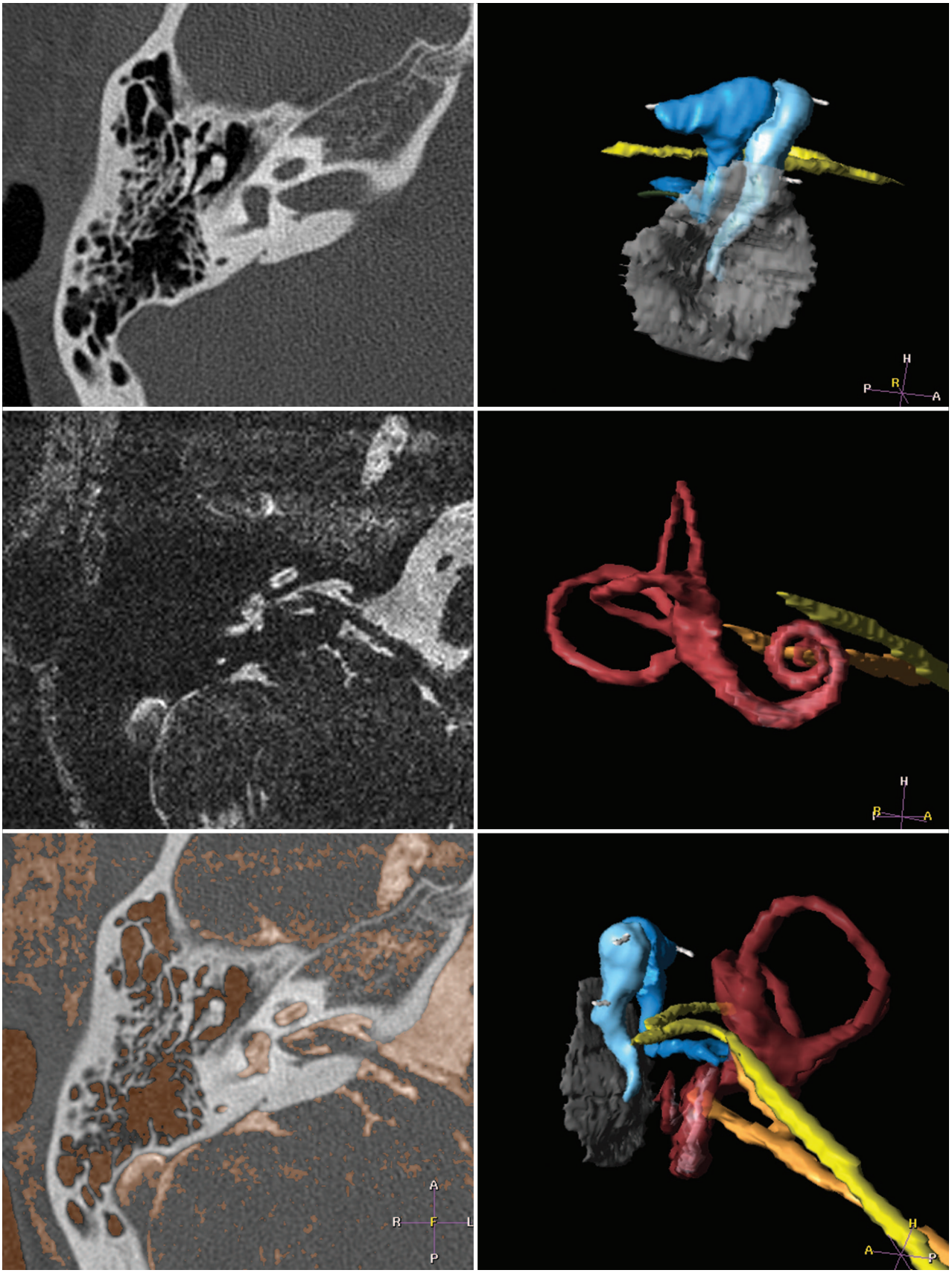

Fig. 1. Normal right middle and inner ear of a 18-year-old woman with tinnitus. (A) Axial HR-CT source image of the petrous bone at the level of the malleus and incus using 16-slice computed tomography. (B) Lateral view of the color-coded shaded-surface rendering reconstruction of the middle ear structures [malleus (blue) and incus (dark blue) with their ligamentous suspensions (white), stapes (light blue), membrana tympani (grey), intraosseous part of the facial nerve (yellow), M. stapedius (brown)]. (C) Axial HR-MRI source image of the petrous bone at the level of the cochlea using a 3D-CISS sequence at 3.0 Tesla scanner. (D) Lateral view of the color-coded shaded-surface rendering reconstruction of the inner ear structures [vestibulocochlear apparatus (semicircular canals, vestibulum and cochlea (red) with basilar membrane (blue)) and cranial nerves (facial nerve (yellow) and vestibulocochlear nerve (orange)) within the internal auditory canal (IAC) and the cerebellopontine angle (CPA)]. (E) Image fusion of source images from HR-CT and HR-MRI and (F) from the color-coded shaded-surface rendering reconstructions.

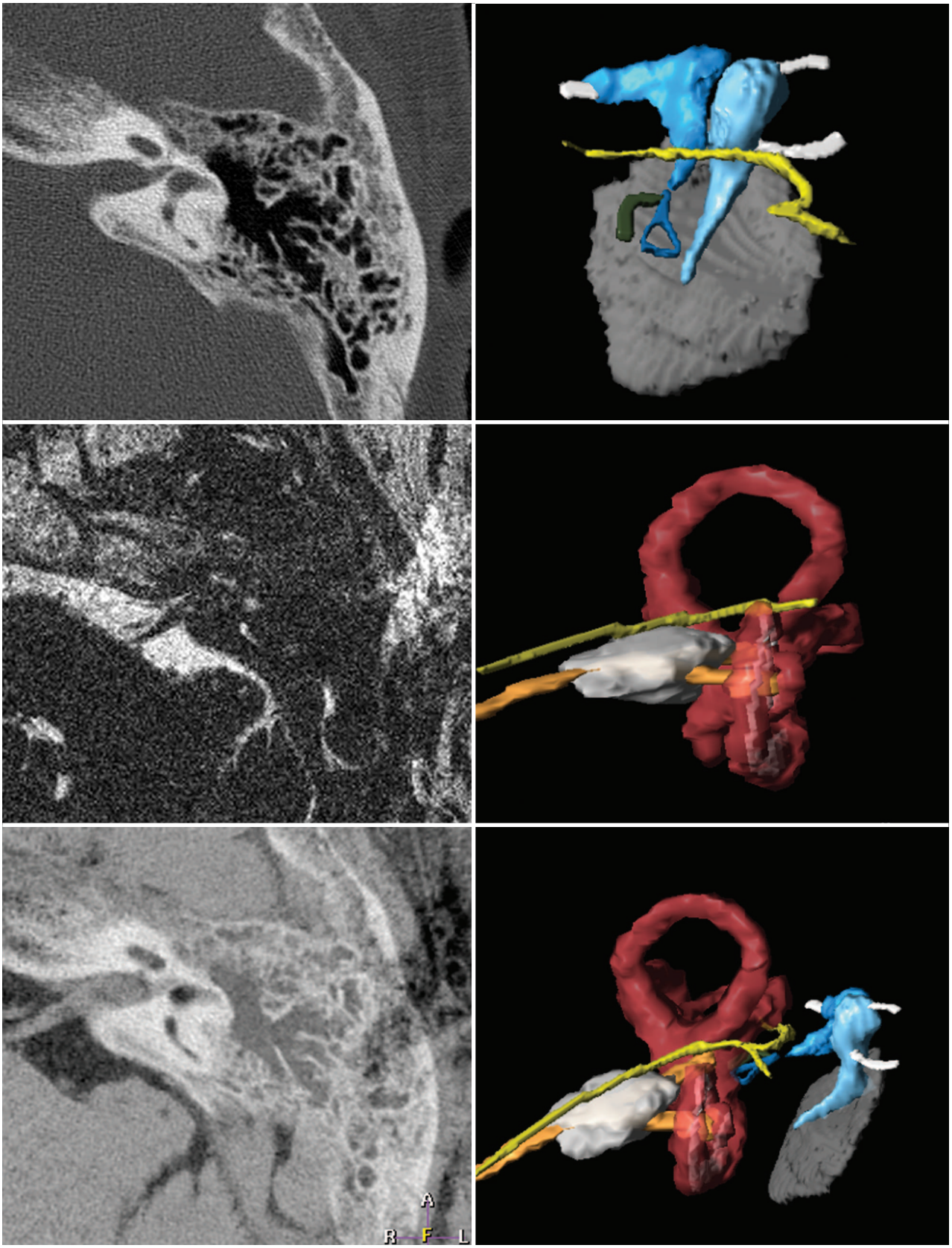

Fig. 2. Intracanalicular acoustic schwannoma of the eight cranial nerve of the left inner ear in a 63-year-old woman with vertigo. There are no erosions of the bony porus and IAC walls on the HRCT. (A) Axial HR-CT source image of the petrous bone at the level of the malleus and incus using 16-slice computed tomography. (B) Lateral view of the color-coded shaded-surface rendering reconstruction of the middle ear structures [malleus (blue) and incus (dark blue) with their ligamentous suspensions (white), stapes (light blue), membrana tympani (grey), intraosseous part of the facial nerve (yellow), M. stapedius (brown)]. (C) Axial HR-MRI source image of the petrous bone at the level of the cochlea using a 3D-CISS sequence at 3.0 Tesla scanner. (D) Lateral view of the color-coded shaded-surface rendering reconstruction of the inner ear structures [vestibulocochlear apparatus (semicircular canals, vestibulum and cochlea (red) with basilar membrane (blue)) and cranial nerves (facial nerve (yellow) and vestibulocochlear nerve (orange)) within the internal auditory canal (IAC) and the cerebellopontine angle (CPA)] and the intracanalicular acoustic schwannoma (gray). (E) Image fusion of source images from HR-CT and HR-MRI and (F) from the color-coded shaded-surface rendering reconstructions.

Table 2. Qualitative assessment of the representation and spatial orientation of the middle and inner ear structures (n = 20) in the fused axial CT/MRI compared with the fused color-coded SSD CT/MRI (consensus readings).

	axial CT/MRT fusion representation	3D CT/MRT fusion representation	axial CT/MRT fusion spatial orientation	3D CT/MRT fusion spatial orientation
Middle ear structures				
malleus	+ + +	+ + +	+ +	+ + +
incus	+ + +	+ + +	+ +	+ + +
stapes	+ + +	+ + +	+ +	+ + +
Inner ear structures				
superior semicircular canal	+ + +	+ + +	+ +	+ + +
lateral semicircular canal	+ + +	+ + +	+ +	+ + +
posterior semicircular canal	+ + +	+ + +	+ +	+ + +
vestibule	+ + +	+ + +	+ +	+ + +
cochlea	+ + +	+ + +	+ +	+ + +
basilar membran				
facial nerve				
part in the IAC and CPA	+ + +	+ + +	+ +	+ + +
part in the petrous bone	+ +	+ + +	+ +	+ + +
vestibulocochlear nerve	+ + +	+ + +	+ +	+ + +

Note.—Each case was read using a score from 0 to + + + (0 = not visible, + = insufficient, + + = fair, + + + = optimal).

image post-processing. High-resolution computed tomography (HR-CT) is the modality of choice for the imaging and evaluation of the fine bony architecture of the middle and inner ear [7], while high-resolution magnetic resonance imaging (HR-MRI) is the modality of choice for the imaging and evaluation of the fluid-filled spaces, soft tissue structures, nerval structures and tumor staging of the middle and inner ear. Therefore, to realistically depict the diagnostic, anatomical and pathological information of the auditory and vestibular system, data sets from both HR-CT and HR-MRI are required. In comparison to the axial 2D source images, 3D image post-processing provides an excellent overview and an improved representation of the complex spatial relationships of the individual anatomical and pathological features of the middle and inner ear structures [1].

CT is the method of choice for accurate visualization and assessment of the status of the ossicles of the middle ear and the osseous boundaries of the external (EAC) and internal auditory canal (IAC), and the middle and inner ear [3, 4]. For clarification of the auditory and vestibular system, scanning of thin sections with high spatial resolution and special reconstruction software is necessary. HR-CT allows enhancement of bone details and makes it possible to delineate the tympanic membrane, the bony microanatomy (defects, displacement and erosions of the ossicles and the suspensory ligaments), microcalcifications (tympanosclerosis) or ossification (new bone formation) of soft tissues in the middle ear, as well as enabling the detection of middle ear and mastoid pneumatization, traumatic changes (ossicular chain and temporal bone fractures) and intraosseus pathologies [8, 9]. Therefore, CT is the primary modality for the study of patients with keratosis obturans, otosclerosis, otodystrophies, chronic otitis media and cholesteatoma. A pre-operative CT provides important details about potential surgical routes intended to drain or resect lesions, and to assess any aberrance in the course of the facial nerve before any surgical attempt to restore hearing [4, 10-13]. CT is also the method of choice to evaluate the postoperative middle ear and mastoid, to detect granuloma or fibrous tissue formation, recurrent otosclerosis, prosthesis subluxation, incus necrosis or dislocation and fistula. In most cases, it is impossible, however, to distinguish between mucosa, fluid, cholesteatoma, granulation tissue, neoplasms, fibrosis, and surgical scarring and packing with CT, even when measurements of densities are used [4].

In recent years, MR imaging has proven to be the imaging method of choice for the assessment of soft-tissue structures and fluid-containing structures of the middle and inner ear, and it also has proven valuable in the study of tumors of the temporal bone [3, 4, 14-17]. For investigation of the auditory and vestibular system, routine MR sequences include (1) selective three-dimensional Fourier transformation (3DFT) high-resolution gradient-echo images, (2) unenhanced and (3) gadolinium (Gd)-enhanced T1-weighted (T1w) spin-echo (SE) or turbo spin-echo (TSE) images through the temporal bone and (4) T2-weighted (T2w) spin-echo (SE) or turbo spin-echo (TSE) images of the brain and brain stem [3]. T2w-SE images have to be obtained prior to the administration of Gd to avoid Gd-intensified flow artifacts [3]. MR data acquisition of fluid-filled spaces of the inner ear is achieved by high-resolution, heavily T2-weighted sequences, typically including a fast spin-echo (FSE) or gradient echo 3DFT-constructive interference in steady state (3DFT-CISS) sequence [15, 18]. Numerous studies have demonstrated the high contrast of very small struc-

tures and the excellent performance of 3DFT-CISS to produce images depicting of subtle pathologic changes of the inner ear and the cranial nerves within the internal auditory canal (IAC) and the cerebellopontine angle (CPA) [2, 6, 18-20]. Some authors preferred the FSE technique, because of reduced signal loss due to susceptibility effects [15, 21]. The advent of 3DFT-CISS sequences enabled the imaging of many structures that were previously not visible. The facial nerve, the three branches of the vestibulocochlear nerve inside the internal auditory canal, the anterior inferior cerebellar artery (AICA) loop in the cerebellopontine angle and internal auditory canal, the scala tympani and vestibuli in the different cochlear turns, the vestibule with the utricular nerve, the semicircular ducts and their ampullae, the fluid in the endolymphatic sac and duct, and the vessels in the subarcuate canal are some structures that can now be visualized in a reliable manner [18]. The high-resolution T2-weighted gradient-echo (3D-CISS) images are able to reliably detect the narrowing of the cochlea and intralabyrinthine fluid spaces, congenital inner ear malformations, vestibulocochlear nerve hypoplasia or aplasia, as well as showing the relationship of the vessels to the nerves when a vascular compression of the vestibulocochlear nerve is suspected and to diagnose fibrous obliteration of the inner ear [7, 18]. The unenhanced T1w-sequences are the method of choice to visualize the labyrinthine, tympanic and mastoid segment of the facial nerve and the greater superficial petrosal nerve and to recognize hyperintensity inside the labyrinth caused by the presence of blood (trauma-labyrinthitis-cholesterol granuloma), fat (lipoma) or increased protein (schwannoma). A subtle increase in signal intensity in cases of schwannoma is a reliable sign aiding in the differentiation with neuritis. The Gd-enhanced T1w-sequences are the modality of choice, not only for the evaluation of small tumors in the cerebellopontine angle and internal auditory canal [11, 22, 23], but also for the reliable detection of tumors (meningioma, schwannoma, metastasis, lymphoma, glioma, melanoma, epidermoid, arachnoid cyst), vascular lesions or tumors (vertebrobasilar dolichoectasia, sigmoid sinus thrombosis, vascular loops, aneurysms, hemangioma), inflammatory processes (cholesteatoma (also residual and recurrent disease), labyrinthitis, neuritis, meningitis, epidural and brain abscess), traumatic changes (perilymphatic fistulas and damaged facial nerve segment), meningeal hyperemia or invasion, subarachnoid seeding and intracranial and intracerebral extension of diseases [14, 24-26]. The T2w-sequences are most sensitive for visualization of peritumoral edema, peritumoral arachnoid cyst formation and facial nerve lesions at the nuclear or supranuclear level [2, 3, 17, 18]. They are used to reliably exclude vertebrobasilar ischaemia and demyelinating disease in the brain, auditory cortex, brain stem and cerebellum and to further characterize tumors or bone lesions. Inspite of this, MRI is relatively insensitive to the presence of ossicular abnormalities and subtle bone erosions and calcifications. Imaging problems of the inner ear have arisen from incomplete data acquisition, motion and pulsation artifacts (internal carotid, basilar and vertebral arteries), fluid-retaining mastoid cells close to the inner ear and post-operative signal alterations [27].

CT and MR imaging are complementary in patients with inner ear malformations, such as syndromal inner ear dysplasia with associated middle ear pathology, or in cases in which high grade bony inner ear obliteration prevents the differentiation of dysplasia from post-inflammatory obliteration, or in the assessment of sensorineural hearing loss [3, 27-29]. The imaging methods are also complementary for the differentiation between congenital aplasia and labyrinthitis ossificans and between fibrous and calcified obliteration in patients requiring cochlear implants [2], as well as in the adequate examination of the complex course of the facial (seventh) nerve from the cerebellopontine angle to the final division [7, 30]. Both imaging methods are often required in the preoperative differentiation of solid tumors (meningioma, hemangioma and schwannoma) and the determination of the involved anatomical structures and the extension of disease. CT may show calcifications (subtle in case of chordoma and larger in case of chondrosarcomas) and detect subtle bony changes, and therefore, provides more information when tumor lesions are small and confined to the middle ear and possible surgical routes must be evaluated. The primary role of MR imaging is to study large lesions, lesions of the outer ear and the skull base, lesions completely confined to the soft tissues and the invasion of lesions to adjacent soft tissue and brain [31, 32]. CT and MRI are complementary in recurrent SNHL or vertigo in patients with prosthesis, because CT can demonstrate abnormal penetration of the prosthesis in the labyrinth, a pneumolabyrinth, or ossification of the labyrinth, whereas MRI is more reliable in detecting acute labyrinthitis, intravestibular fibrosis formation, and Gd-enhancement inside of the labyrinth in cases of a perilymph fistula [24].

Since the structures of the middle and inner ear are oriented three-dimensionally, data acquisition has to be taken in more than one plane for a thorough evaluation, because no single orientation allows comprehensive the optimal evaluation of these structures [4]. The commonly used axial slices allow the patient to lie comfortably during data acquisition and allows the examiner a better comparison with the contralateral temporal bone. Nevertheless, the axial image representation is not ideal for understanding the 3D anatomy and abnormalities, and pathological findings can make their interpretation more complicated. There are different data post-processing techniques to visualize the middle and inner ear. The maximum intensity projection (MIP) from 3D CISS sequence reduces the complex 3D inner ear structures to various 2D projection images and produce a pseudo 3D visualization of the inner ear and their malformations, which lacks important depth information [2]. There are two fundamentally different methodical approaches for generating 3D image processing, which also form the basis of virtual endoscopy. These are the surface rendering and the volume rendering approach [33, 34]. In surface rendering, the image information of the volume data set is provided with a weighting related to the importance of the defined and segmented structures of interest. This method requires an operator for the seg-

mentation in order to create the surface models. The volume rendering method preserves all the image information of the whole CT volume data set by facilitating direct 3D visualization of the volume data set.

Conclusion

Computed tomography (CT) and magnetic resonance imaging (MRI) are complementary imaging modalities in the visualization of anatomical findings and pathological changes of the auditory and vestibular system. CT is superior to MRI in assessing fine bony details and in identifying microcalcifications. MRI is superior to CT in evaluating soft tissue and fluid-filled spaces and provides the option of imaging the brain stem and the auditory cortex [2, 3, 10, 17, 18]. Therefore, a realistic and individual depiction of the complex anatomical relationships requires a 3D image fusion of HR-CT and HR-MRI data sets. High quality 3D image fusion data processing provides the necessary diagnostic information without detailed analysis and presentation of axial source images of different imaging modalities and will increase the acceptance and diagnostic value of HR-CT and HR-MRI for middle and inner ear diseases in the clinical practice.

References

1. Seemann MD, Seemann O, Bonél H, et al. (1999) Evaluation of the middle and inner ear structures: comparison of hybrid rendering, virtual endoscopy and axial 2D source images. Eur Radiol 9: 1851-1858.
2. Casselman JW, Kuhweide R, Ampe W, et al. (1996) Inner ear malformations in patients with sensorineural hearing loss: Detection with gradient-echo (3DFT-CISS) MRI. Neuroradiology 38: 278-286.
3. Casselman JW (1996) Temporal bone imaging. Neuroimaging Clin North Am 6: 265-289.
4. Shankar L, Montanera W (1991) Computed tomography versus magnetic resonance imaging and three-dimensional applications. Med Clin North Am 75: 1355-1366.
5. Swartz JD, Swartz NG, Korsvik H, et al. (1985) Computerized tomographic evaluation of the middle ear and mastoid for posttraumatic hearing loss. Ann Otol Rhinol Laryngol 94: 263-266.
6. Casselman JW, Kuhweide R, Dehaene I, Ampe W, Devlies F (1994) Magnetic resonance examination of the inner ear and cerebellopontine angle in patients with vertigo and/or abnormal findings at vestibular testing. Acta Otolaryngol 513 (Suppl.): 15-27.
7 Liu DP, Bergeron RT (1989) Contemporary radiologic imaging in the evaluation of middle ear-attic-antral complex cholesteatomas. Otolaryngol Clin North Am 22: 897-909.
8. Shaffer KA (1984) Comparison of computed tomography and complex motion tomography in the evaluation of cholesteatoma. Am J Roentgenol 143: 397-400.
9. Virapongse C, Rothman SL, Kier EL, Sarwar M (1982) Computed tomographic anatomy of the temporal bone. Am J Roentgenol 139: 739-749.
10. Jackler RK, Parker DA (1992) Radiographic differential diagnosis of petrous apex lesions. Am J Otol 13: 561-574.
11. Phelps PD, Lloyd GA (1989) Magnetic resonance with gadolinium DTPA for the investigation of temporal bone tumors. Otolaryngol Clin North Am 14: 251-262.
12. Seemann MD, Luboldt W, Haferkamp C, et al. (2000) Hybrid rendering and virtual endoscopy in cochlear implants. Fortschr Röntgenstr 172: 238-243.
13. Shankar L, Hawke M, Leekam RN, Rutka J (1989) Computed tomographic analysis of the intratemporal facial nerve and facial nerve neuromas. Can Assoc Radiol J 40: 150-155.
14. Casselman JW, Kuhweide R, Ampe W, Meeus L, Steyaert L (1993) Pathology of the membranous labyrinth: comparison of T1- and T2-weighted and gadolinium-enhanced spin-echo and 3DFT-CISS imaging. Am J Neuroradiol 14: 59-69.
15. Harnsberger HR, Dahlen RT, Shelton C, Gray SD, Parkin JL (1995) Advanced techniques in magnetic resonance imaging in the evaluation of the large endolymphatic duct and sac syndrome. Laryngoscope 105: 1037-1042.
16. Mafee MF, Kumar A, Heffner DK (1994) Epidermoid cyst (cholesteatoma) and cholesterol granuloma of the temporal bone and epidermoid cysts affecting the brain. Neuroimaging Clin North Am 4: 561-578.
17. Swartz JD (1996) Sensorineural hearing deficit: A systematic approach based on imaging findings. Radiographics 16: 561-574.
18. Casselman JW, Kuhweide R, Deimling M, Ampe W, Dehaene I, Meeus L (1993) Constructive interference in steady state-3DFT MR imaging of the inner ear and cerebellopontine angle. Am J Neuroradiol 14: 47-57.
19. Graf H, Schick F, Claussen CD, Seemann MD (2004) MR visualization of the inner ear structures: comparison of 1.5 Tesla and 3 Tesla images. Fortschr Rontgenstr 176: 17-20.
20. Klingebiel R, Thieme N, Werner JF, et al. (2001) A postprocessing protocol for three-dimensional visualization of the inner ear using the volume-rendering technique based on a standard magnetic resonance imaging protocol. Acta Otolaryngol 121: 384-386.
21. Naganawa S, Yamakawa K, Fukatsu H, et al. (1996) High-resolution T2-weighted MR imaging of the inner ear using a long echo-train-length 3D fast spin-echo sequence. Eur Radiol 6: 369-374.
22. Gentry LR, Jacoby CG, Turski PA, Houston LW, Strother CM, Sackett JF (1987) Cerebellpontine angle-petromastoid mass lesions: comparative study of diagnosis with MR imaging and CT. Radiology 162: 513-520.
23. Hasso AN, Smith DS (1989) The cerebellopontine angle. Semin Ultrasound CT MR 10: 280-301.
24. Mark AS, Fitzgerald D (1993) Segmental enhancement of the cochlea on contrast-enhanced MR: correlation with the frequency of hearing loss and possible sign of perilymphatic fistula and autoimmune labyrinthitis. Am J Neuroradiol 14: 991-996.
25. Martin N, Sterkers O, Nahum H (1990) Chronic inflammatory disease of the middle ear cavities: Gd-DTPA-enhanced MR imaging. Radiology 176: 399-405.
26. Mulkens TH, Parizel PM, Martin JJ, et al. (1993) Acoustic schwannoma: MR findings in 84 tumors. Am J Roentgenol 160: 395-398.
27. Klingebiel R, Bockmühl U, Werbs M, et al. (2001) Visualization of inner ear dysplasias in patients with sensorineural hearing loss. High-resolution MR imaging and volume-rendered reconstructions. Acta Radiologica 42: 574-581.
28. Antonelli PJ, Varela AE, Mancuso AA (1999) Diagnostic yield of high-resolution computed tomography for pediatric sensorineural hearing loss. Laryngoscope 109: 1642-1647.
29. Bamiou DE, Savy L, O´Mahoney C, Phelps P, Sirimanna T (1999) Unilateral sensorineural hearing loss and its aetiology in childhood: The contribution of computerised tomography in aetiological diagnosis and management. Int J Pediatr Otorhinolaryngol 51: 91-99.
30. Holliday RA (1989) Inflammatory diseases of the temporal bone: evaluation with CT and MR. Semin Ultrasound CT MR 10: 213-235.

31. Castillo M, Harold CP (1992) Rhabdomyosarcoma of the middle ear: imaging features in two children. Am J Neuroradiol 14: 730-733.
32. Friedman DP, Rao VM. MR and CT of squamous cell carcinoma of the middle ear and mastoid complex. Am J Neuroradiol 1991; 12: 872-874.
33. Seemann MD, Seemann O, Englmeier KH, Allen CM, Haubner M, Reiser MF (1998) Hybrid rendering and virtual endoscopy of the auditory and vestibular system. Eur J Med Res 3: 515-522.
34. Udupa JK, Hung HM, Chuang KS (1991) Surface and volume rendering in three-dimensional imaging: a comparison. J Digit Imaging 4: 159-568.

Received: January 11, 2005 / Accepted: February 14, 2005

Address for correspondence:
Marcus D. Seemann, M. D.
Associate Professor of Radiology
Department of Nuclear Medicine
Technical University, Munich
Ismaninger Strasse 2 2
D-81675 Munich, Germany
Tel. +49-89/41402971
Fax +49-89/41404841
e-mail: m.seemann@lrz.tum.de